

Bioavailability of Gold Nanomaterials to Plants: Importance of Particle Size and Surface Coating

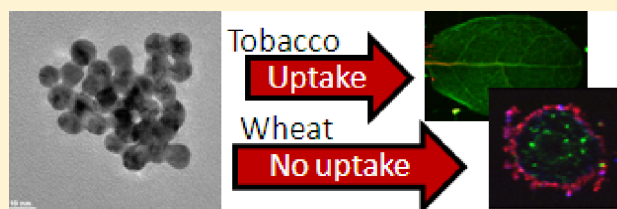
Jonathan D. Judy,[†] Jason M. Unrine,[†] William Rao,[†] Sue Wirick,^{†,‡} and Paul M. Bertsch^{*,†}

[†]Department of Plant and Soil Sciences, University of Kentucky, Lexington, Kentucky 40546, United States

[‡]Center for Advanced X-ray Sources (CARS), University of Chicago, Chicago, Illinois 60637, United States

S Supporting Information

ABSTRACT: We used the model organisms *Nicotiana tabacum* L. cv *Xanthi* (tobacco) and *Triticum aestivum* (wheat) to investigate plant uptake of 10-, 30-, and 50-nm diameter Au manufactured nanomaterials (MNMs) coated with either tannate (T-MNMs) or citrate (C-MNMs). Primary particle size, hydrodynamic size, and zeta potential were characterized using transmission electron microscopy (TEM), dynamic light scattering (DLS), and electrophoretic mobility measurements, respectively. Plants were exposed to NPs hydroponically for 3 or 7 days for wheat and tobacco, respectively. Volume averaged Au concentrations were determined using inductively coupled plasma mass spectrometry (ICP-MS). Spatial distribution of Au in tissue samples was determined using laser ablation ICP-MS (LA-ICP-MS) and scanning X-ray fluorescence microscopy (μ XRF). Both C-MNMs and T-MNMs of each size treatment bioaccumulated in tobacco, but no bioaccumulation of MNMs was observed for any treatment in wheat. These results indicate that MNMs of a wide range of size and with different surface chemistries are bioavailable to plants, provide mechanistic information regarding the role of cell wall pores in plant uptake of MNMs, and raise questions about the importance of plant species to MNM bioaccumulation.



■ INTRODUCTION

Manufactured nanomaterials (MNMs) are being discharged into waste streams from the rapidly increasing number of consumer products that employ nanotechnology.^{1–3} Studies have consistently demonstrated that MNMs concentrate in the sludge during wastewater treatment,^{1,3–5} 60% of which is applied to agricultural land as biosolids in the U.S. and the majority of Europe.¹ As a result, the MNM concentrations in sludge-treated soil in the U.S. are expected to rise rapidly.¹ A recent model conservatively predicted increases from 0.1 to 0.5 mg kg⁻¹ for TiO₂ MNMs, from 6.8 to 22.3 μ g kg⁻¹ for ZnO MNMs, and from 2.3 to 7.4 μ g kg⁻¹ for Ag MNMs between 2008 and 2012.¹ Despite this, little is known about the bioavailability and toxicity of sludge-accumulated MNMs to plants and other terrestrial organisms following their introduction into the soil.⁶

In the past few years, many studies have investigated plant uptake of a wide variety of MNMs in many different plant species. For example, early studies demonstrated the uptake of uncoated 20-nm Fe₃O₄ MNMs by pumpkin plants,⁷ uncoated 50-nm Cu MNMs by wheat and mungbean,⁸ and natural organic matter (NOM) coated 1.19-nm C₇₀ fullerenes by rice.⁹ More recent research has demonstrated the uptake of alizarin red and sucrose coated 2.8-nm TiO₂ MNMs by *Arabidopsis thaliana*,¹⁰ 15-nm tannate coated and 3.5-nm citrate coated Au MNMs by *Nicotiana tabacum*,^{11,12} and of 6-nm gum arabic coated silver MNMs by *Lolium multiflorum*.¹³ Conversely, many studies investigating plant uptake of MNMs have reported no uptake. For example, researchers reported no

uptake of uncoated 19-nm ZnO MNMs by ryegrass,¹⁴ no uptake of uncoated 37-nm CeO₂ MNMs by maize,¹⁵ and no uptake of uncoated 20-nm TiO₂ or uncoated 40-nm ZnO by wheat.¹⁶ Many of these studies have been published without adequate MNM characterization or investigation of the localization of MNMs within cells or tissues. Without measurements to establish MNM localization, it can be difficult to eliminate the possibility that reported bioaccumulation is simply reflective of MNMs or dissolved species on the exterior surfaces of the plants.⁶

The majority of these studies exposed a single plant species to one MNM treatment or to several different types of MNMs. There have been few studies that have attempted to systematically evaluate the relative importance of particle characteristics or plant species on plant bioaccumulation of MNMs. There is a fundamental difference in the nature of root exudates between monocots and dicots, as these groups have different strategies for obtaining metal nutrients from the soil.¹⁷ Therefore, it is reasonable to hypothesize that differences in type and amount of root exudates between plant species might also affect uptake, either by facilitating uptake or by inducing MNM aggregation. Furthermore, each MNM has intrinsic properties that may affect mobility, bioavailability, or toxicity, as well as the likely transformations it will undergo in the

Received: May 14, 2012

Revised: July 10, 2012

Accepted: July 11, 2012

Published: July 11, 2012

environment. These properties include composition, crystal structure, size, shape, and surface chemistry.^{18–21} Nanomaterial size is likely to be important to MNM bioaccumulation in plants as plant cell wall pores have been shown to be size selective to macromolecules.²² Nanomaterial surface chemistry is likely to be an important factor in plant uptake as plant cell surfaces will present barriers of varying hydrophobicity and surface charge.¹⁷

We recently demonstrated plant uptake, trophic transfer, and biomagnification of Au MNMs.¹² Considering these results and the fact that plants comprise the base of many terrestrial food webs, there is an urgent need to systematically characterize the factors that control the bioavailability of MNMs to plants. To begin addressing this need, we used the model organisms *Nicotiana tabacum* L. cv *Xanthi* and *Triticum aestivum* to investigate plant uptake of 10-, 30-, and 50-nm diameter tannate (T-MNMs) or citrate (C-MNMs) coated Au MNMs.¹² The objectives of the study were to systematically investigate the importance of MNM size between the range of 10 and 50 nm in plant bioaccumulation of MNMs, to collect data elucidating the importance of MNM surface chemistry on plant bioaccumulation of MNMs, and to collect data clarifying the importance of plant species to plant bioaccumulation of MNMs.

■ EXPERIMENTAL SECTION

Nanoparticle Characterization. Stable suspensions of 10-, 30-, and 50-nm diameter primary particle size Au MNMs surface modified with either tannate (Nanocomposix San Diego, CA, USA) or citrate (Ted Pella, Redding, CA, USA) were purchased and the stock suspensions were characterized using transmission electron microscopy (TEM, see Supporting Information (SI), Table S1). Au MNMs are being used in applications including medical imaging,²³ drug delivery,²⁴ and fuel cell catalysis.²⁵ We selected Au MNMs for this study due to their resistance to oxidative dissolution and low natural background concentrations. These properties make Au MNMs an idea probe for investigating MNM bioaccumulation and translocation.²⁶ Tannate is a high molecular weight polyphenol with a log K_{ow} of -0.19 ²⁷ with $pK_{a1} = 4.4$ ^{28,29} and $pK_{a2} = 10$.³⁰ Citrate is a low molecular weight organic acid with log K_{ow} of -1.74 ³¹ with $pK_{a1} = 3.1$, $pK_{a2} = 4.7$, and $pK_{a3} = 5.4$.³² Tannate and citrate coated MNMs were selected for this study because we consider these two molecules to be reasonable analogues for common low molecular weight organic acids found in soil and high molecular weight NOM complexes, respectively, both of which we envision could adsorb to MNMs in the soil as is often observed for fine-grained soil mineral surfaces.^{33,34} The suspension concentrations were verified through aqua regia digestion and elemental analysis via inductively coupled plasma mass spectrometry (ICP-MS) using an Agilent 7500cx ICP-MS (Agilent, Santa Clara, CA, USA). To determine the concentration of dissolved Au in the stock suspensions, samples of the stock suspensions were filtered through a 3 kDa regenerated cellulose membrane (Amicon Ultra, Millipore, Billerica, MA, USA), after which the resulting filtrate was analyzed for Au using ICP-MS (see Table S1). Measurement of the amount of dissolved Au present in suspension filtrates reveals very low concentrations that are mostly below detection (detection limit = 1.37 ng Au mL; see Table S1). A solution of $10 \mu\text{g L}^{-1}$ HAuCl₄ was filtered through one of the membrane filters used to estimate dissolved Au and a recovery of 82.4%

was determined, which we have found to be a typical recovery at low concentrations, presumably due to interactions with trace functional groups associated with the membranes. Additional details of MNM characterization, including TEM data, are located in the SI.

TEM size analysis of the T-MNMs was provided by the manufacturer (Nanocomposix San Diego, CA, USA) using a Jeol 1010 TEM. The size of the C-MNMs was derived from TEM images collected using a Jeol 2010 TEM. Mean MNM diameter and size ranges were quantified based on measurements of at least 100 individual particles using ImageJ software.

Nanoparticle Treatment Preparation. Prior to dilution to 30 mg L^{-1} , MNMs were treated to purify the MNM suspensions, buffer the solution to prevent destabilization of the coating, and to attempt to homogenize the pH and electrophoretic mobilities of each MNM treatment. The C-MNMs were washed with a pH 7 sodium citrate–citric acid buffer of a concentration normalized to the surface area of each treatment. For the 10-, 30-, and 50-nm MNMs, a 1 mM, 0.4 mM, and 0.33 mM buffer was used, respectively. All three T-MNM treatments were diluted to 30 mg L^{-1} with 0.1 mM tannic acid and adjusted to pH 7 with dilute NaOH. T-MNMs were not stable at higher concentrations of tannic acid, possibly due to the relatively high molecular weight of tannic acid, so it was not possible to use the same approach as was used with the C-MNMs. The T-MNMs had been washed 10 times with $18 \text{ M}\Omega \text{ cm}^{-1}$ deionized water (DI) by the manufacturer prior to purchase. Mean intensity weighted hydrodynamic diameters and electrophoretic mobilities of the exposure suspensions were measured with a Nano-ZS zetasizer (Malvern, Worcestershire, UK) using 173° backscatter analysis method. Hydrodynamic diameter distributions were converted to a volume basis using a refractive index of 0.2 and absorption of 3.32 (see Table S2). All MNM treatment suspensions were highly negatively charged with zeta potentials $> -50 \text{ mV}$ (see Table S2). Electrophoretic mobilities were converted to zeta potentials using the Hückel model.

Plant Exposure Protocol. *Nicotiana tabacum* L. cv *Xanthi* was selected as a model primary producer for this study due to its demonstrated ability to bioconcentrate metals,³⁵ whereas *Triticum aestivum* was selected as a model organism for this experiment because it is an important food crop. Germination and growth methods for both tobacco and wheat are described in the SI. At 30 days post germination for tobacco and 7 days post germination for wheat, plants were randomly divided into treatment populations and placed in 1.5-mL microcentrifuge tubes. We elected to perform a hydroponic exposure over a soil exposure because we believe that it would be virtually impossible to separate the importance of intrinsic particle properties to plant uptake from the importance of extrinsic properties imparted by soil components to uptake. Fifteen plants were exposed to each of the six treatment combinations. Controls consisted of 5 plants each in DI, 1 mM pH 7 sodium citrate–citric acid buffer, and pH 7 0.1 mM tannic acid. Treatment solutions were periodically adjusted to the initial volume with the appropriate buffer. Since wheat does not tolerate nutrient stress as well as tobacco due to differences in its growth and development, tobacco plants were exposed for 7 days whereas wheat plants could only be exposed for 3 days. Plant growth over the exposure period appeared negligible.

Sample Collection and Preparation. At the end of each exposure, plant roots were cut from each plant above the level of the MNM suspensions to remove tissue that might have

been surface contaminated with MNMs. The aerial portion of each plant was carefully washed with DI, citranox, 0.5% HCl/0.5% HNO₃, and then again with DI prior to being dried for bulk analysis by ICP-MS. Other leaf samples were mounted on metal free polyimide film for spatially resolved analysis using laser ablation inductively coupled mass spectrometry (LA-ICP-MS) and scanning X-ray fluorescence microscopy (μ XRF). In the wheat exposure, roots were fixed in 10% formalin acetate and subsequently placed in optimal cutting temperature embedding medium (Sankura Finetek, Torrance, CA, USA), frozen using dry ice, and stored at -80°C for later cryo-sectioning to 15 μm thickness for μ XRF analysis.

Post-Exposure Treatment Suspension Characterization. The degree to which the MNMs were aggregated during the wheat and tobacco exposures was characterized through post-exposure sedimentation analysis of the treatment suspensions. One mL of each suspension was vortex mixed thoroughly and then centrifuged at 1100g for 1 min to sediment aggregates larger than approximately 840 nm according to Stoke's law calculations. After collecting a 10- μL sample from the supernatant, the treatment suspensions were vortex mixed again and then centrifuged at 11 000g for 1 min to sediment aggregates larger than approximately 80 nm, after which another 10 μL was removed. As wheat plants have been demonstrated to strongly alkalize their rhizosphere, the post-exposure pH of each treatment suspension from both plants was recorded and Ca and Mg, as well as Au, concentrations were measured using ICP-MS.³⁶ These data will be used to clarify the role of root exudates on any observed treatment aggregation.

Laser Ablation Inductively Coupled Mass Spectrometry (LA-ICP-MS). LA-ICP-MS depth profiles were collected using a series of controlled laser pulses from a LSX-213 laser ablation system (CETAC, Omaha, NE, USA) that removed $400 \times 400 \mu\text{m}^2$ craters. The laser energy and burst duration were calibrated so that these craters were 15 μm deep. The elemental composition of the material removed during each laser pulse was measured using ICP-MS. Calibration standards for analysis consisted of pellets created by spiking dried and finely ground tobacco to a range of concentrations. A calibration curve was created by simple linear regression of the summed counts from the laser bursts within the depth profile for each standard. Semiquantitative sample concentrations were calculated by fitting the summed counts from each sample depth profile to this calibration curve.

Synchrotron X-ray Analysis. Scanning X-ray fluorescence microscopic measurements of Au were collected at the Au L- α_1 emission line (9713 eV) employing beamline X-26A at the National Synchrotron Light Source at Brookhaven National Laboratory (Upton, NY, USA). To correct for interference from the Zn K- β_1 emission line (9572 eV), leaves and root cross sections were mapped at energies above (12 110 eV) and below (11 850 eV) the Au L- α_{III} absorption edge (11 919 eV). The below edge signal was subtracted from the above edge signal and the difference was reported as the Au signal. Additional details of the synchrotron X-ray analysis and beamline configuration are described in the SI.

Inductively Coupled Plasma-Mass Spectrometry Analysis. Plant samples were oven-dried for 48 h at 60°C , weighed, and placed in microcentrifuge tubes. The samples were digested overnight at 60°C in a mixture of 50 μL of hydrogen peroxide and 150 μL of nitric acid. Then, 300 μL of hydrochloric acid was added and the samples were heated for an additional 4 h,

after which the digestate was brought to a 3 mL volume¹² and analyzed by ICP-MS. Analytical runs contained calibration verification samples, duplicate dilutions, and spike recovery samples. As there is no widely available standard reference material containing Au in plants, a laboratory control sample was prepared using finely ground dried tobacco leaves spiked with Au standard to a concentration of 10 mg kg^{-1} . The measured concentrations were 111.7% of the nominal concentration with a standard deviation of 11.5%. Spike recovery averaged 99.2%, and the mean relative percent difference between duplicate dilutions was 5.5%.

Statistical Analyses. All data were tested for normality and homoscedasticity using Shapiro–Wilk's test and Barlett's test, respectively. Data were log transformed if found not to be normally distributed, and then retested. Significant differences between ICP-MS plant bioaccumulation data, LA-ICP-MS bioaccumulation data, and Ca concentrations in the treatment suspensions post exposure were tested using ANOVA and Student–Newman–Keuls (SNK) means comparisons at $\alpha = 0.05$ when data were normal and homogeneously distributed. Significance of non-normal or data with nonhomogenous variance were analyzed using Kruskal–Wallis and Mann–Whitney U-tests at $\alpha = 0.05$. In rare cases, outliers were removed using Grubb's test.

RESULTS AND DISCUSSION

Bulk analysis of the oven-dried aerial tobacco biomass reveals mean Au concentrations between 2.2 and 53.5 mg kg^{-1} (Figure 1). Significant uptake occurred in every treatment combination.

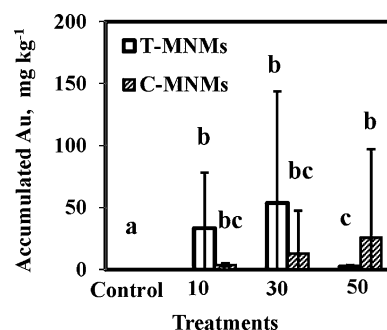


Figure 1. Bulk inductively coupled plasma mass spectrometry (ICP-MS) analysis of tobacco leaf tissue. Error bars represent SD. Treatments with the same letter are not significantly different. T-MNMs = tannate coated manufactured nanomaterials (MNMs); C-MNMs = citrate coated MNMs.

The mean Au concentration in plants exposed to the 50-nm T-MNMs is significantly lower than three of the other treatments but is not significantly different from the 10-nm C-MNM and 30-nm T-MNM treatments. Bulk analysis of the oven-dried aerial biomass reveals no significant uptake in any treatment combination.

The Au concentration in the majority of the tobacco leaf samples determined by scanning X-ray fluorescence is below the estimated detection limit of $\sim 1 \text{ mg kg}^{-1}$ for Au at beamline X-26A. However, one image demonstrates the presence of Au in detectable concentrations in the leaf mid rib of a plant exposed to 30-nm C-MNMs (Figure 2). Images of wheat leaf tissues reveal no evidence of accumulation of Au MNMs in the aerial portions of the plants (see Figure S2). In subtraction maps of root cross sections from the wheat roots, Au MNMs

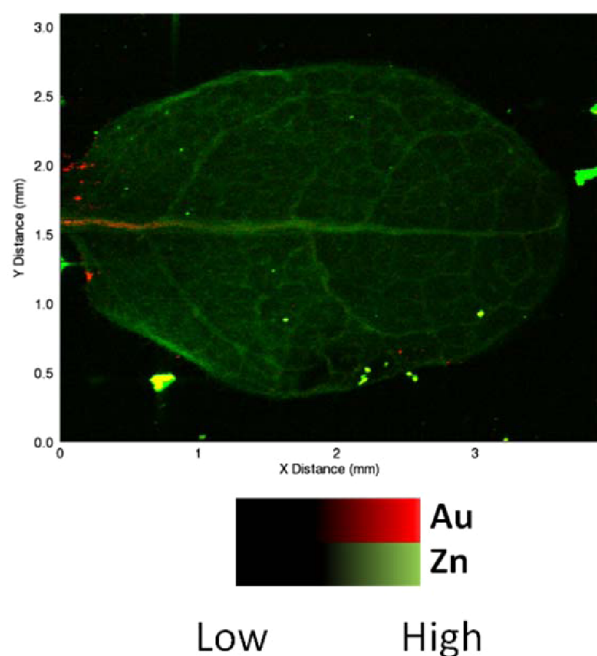


Figure 2. Synchrotron X-ray fluorescence microprobe (μ XRF) map of leaf from a tobacco plant treated with 30-nm citrate coated Au manufactured nanomaterials. Fluorescence from the L- α 1 edge of Au, depicted in red, and K- α 1 edge of Zn, depicted in green. MNMs detected within leaf mid rib near petiole.

are detected adsorbed to the surface of the roots, but there is no evidence that Au MNMs penetrated the root surface in any treatment (Figure 3).

Au is detected by LA-ICP-MS throughout cross sections of tobacco leaves from each treatment (Figure 4). Semi-quantitative Au concentrations determined by LA-ICP-MS are $<1 \text{ mg kg}^{-1}$, consistent with the Au in these samples being below the detection limits of μ XRF imaging at beamline X-26A (Figure 5). Each calibration curve r^2 is >0.999 and there are no significant differences between mean concentrations as a function of MNM treatment or in concentration as a function of cross-section depth in any treatment.

Characterization of the treatment suspensions after exposures demonstrates that, in general, the wheat plants basified their exposure suspensions more than the tobacco plants, although the mean pH for the 30- and 50-nm citrate were similar for the tobacco and wheat samples (see Tables S3 and S4). The results of the sedimentation studies indicate that the MNMs in the wheat exposure suspension aggregated to a greater degree than the MNMs in the tobacco exposures. For example, in the 10-nm tobacco treatments, 61.4% and 67.9% of the T-MNMs and C-MNMs, respectively, were found to be within aggregates larger than 80 nm, compared to 88.3% and 93.3% for the wheat treatments (see Tables S3 and S4). Postexposure analyses of Mg in the treatment suspensions show concentrations mostly below the detection limit ($\sim 1.1 \text{ mg Mg L}^{-1}$ supernatant). Detectable levels of Ca were measured in each treatment for both plant exposures. However, there are no significant differences in mean Ca concentrations based on MNM size, surface coating, or plant species at $\alpha = 0.05$ (see Tables S3 and S4).

This study provides little evidence that primary particle size between 10 and 50 nm is an important factor in plant bioavailability of Au MNMs. We found that bioaccumulation of

50-nm T-MNMs is significantly lower than bioaccumulation of 10- and 30-nm T-MNMs in tobacco. However, this trend was not evident for the C-MNMs and tobacco did accumulate a significant concentration of 50-nm T-MNMs compared to the control. However, it is possible that the large variability in the data set could be masking trends. Although the reasons for this variability are unclear, we speculate that it is in part the result of the large genetic variability among individual tobacco plants. Regardless, this result contradicts the commonly repeated hypothesis that the MNMs must passively pass through cell wall pores to be taken up by plants and that the cell wall will exclude most MNMs larger than 20 nm.^{11,22} The diameter of most cell wall pores have been estimated to be between 5 and 20 nm,^{22,37,38} although recent gas adsorption measurements of cell wall porosity suggest that some cell wall pores may be as large as 50 nm.³⁹ The mechanism by which MNMs might bypass the plant cell wall is not well understood. Studies on fungal cells have demonstrated that Ag MNMs are able to induce plasma membrane depolarization and protoplast leakage suggesting that MNMs can induce pore formation in cell walls in certain cases.⁴⁰ Other studies have provided evidence using confocal microscopy⁴¹ and TEM that clearly demonstrate penetration of the plant cell wall by carbon MNMs.⁴² Another possibility is that minor cuts and other physical damage to the root during the exposure could lead to uptake. Alternatively, Liu et al. demonstrated cellular uptake of single-walled carbon nanotubes by intact tobacco bright yellow (BY-2) cells and reported evidence that endocytosis was the mechanism of uptake.⁴³ The results presented here seemingly contradict our earlier study that used μ XRF mapping to demonstrate that tobacco plants would bioaccumulate 3.5-nm Au MNMs to a greater extent than 18-nm Au MNMs.¹¹ In the earlier study we presented spatial data confirming uptake, but did not provide bulk, volumetrically averaged quantitative analysis, thus the data were only semiquantitative. The present study is not the first to report plant bioaccumulation of larger MNMs. For example, evidence of uptake of magnetite MNMs with a hydrodynamic diameter of approximately 40 nm in pumpkin plants was presented by Zhu et al., although they provided no spatially resolved data.⁷ Lee et al. demonstrated uptake of Cu MNMs with a diameter of approximately 50 nm in mungbean and wheat.⁸

These data do not conclusively demonstrate differences in plant bioaccumulation between the two MNM surface coatings. Although the 50-nm C-MNMs were taken up to a significantly ($\alpha = 0.05$) lesser degree than the 50-nm T-MNMs, this trend did not exist for the 10- and 30-nm MNMs. Considering that tannate and citrate could be considered similar to the NOM coatings that could adsorb to MNM surfaces after introduction into natural ecosystems, this result suggests that MNM coating might be of minor importance in many environmentally relevant scenarios.^{44,45}

The large difference in uptake between the wheat and tobacco suggests that MNMs might be more bioavailable to some plant species than to others. This is consistent with the number of studies presenting both volumetrically averaged and spatially resolved MNM concentrations reporting greater uptake in dicots than in monocots.^{7,8,10–13,16} However, there has been little systematic examination of variation in MNM bioaccumulation based on plant species and there have been reports of positive and negative results in bioaccumulation studies exposing both monocots and dicots. It is possible that the difference in uptake between tobacco and wheat is the

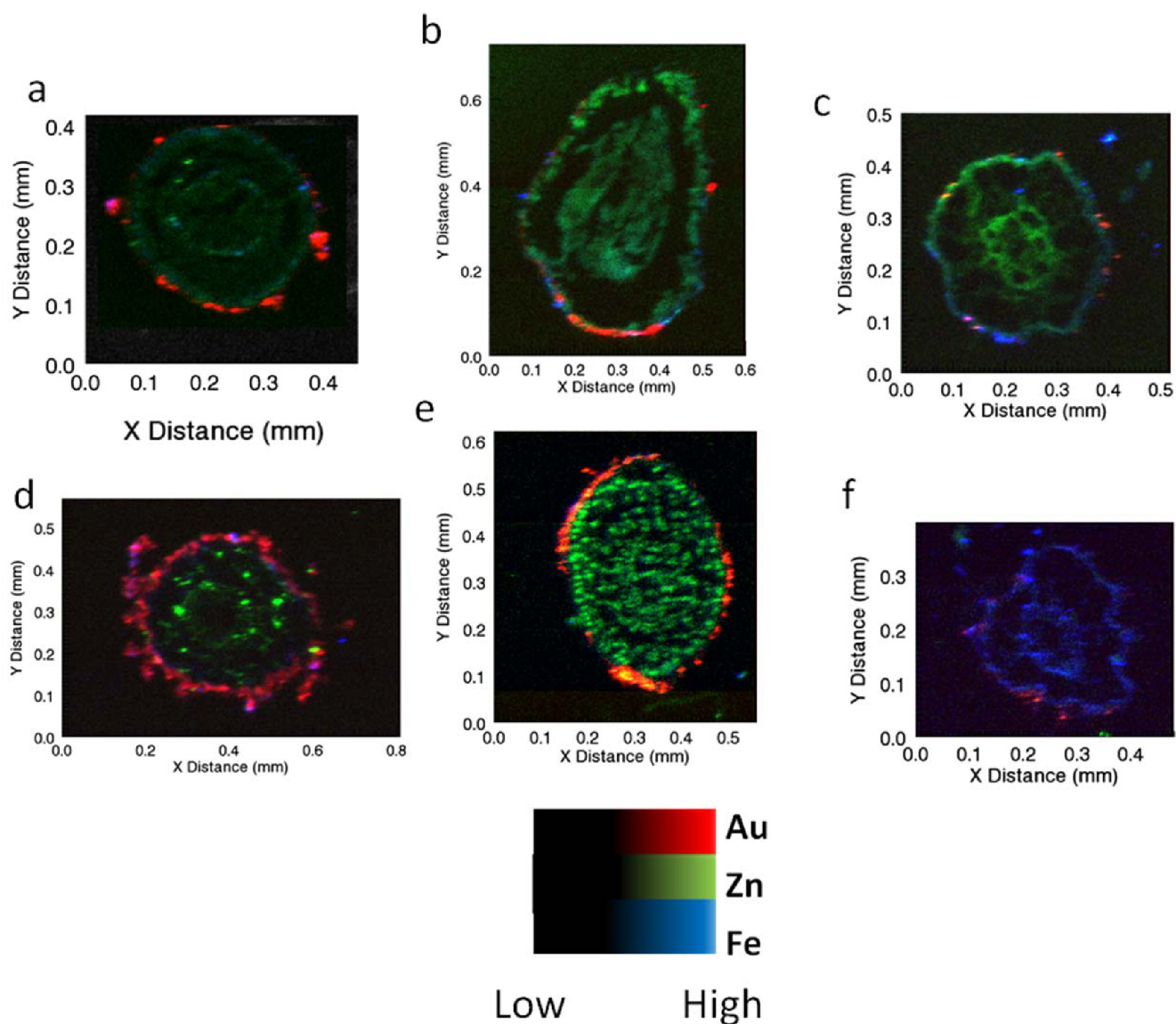


Figure 3. Scanning X-ray fluorescence microscopy (μ XRF) image of fluorescence from the L- α 1 edge of Au, depicted in red, the Zn K- β 1 edge, depicted in green, and the K- α 1 edge of Fe, depicted in blue, for wheat plants exposed to (a) 10-nm, (b) 30-nm, and (c) 50-nm citrate coated manufactured Au nanomaterials (C-MNMS), and (d) 10-nm, (e) 30-nm, and (f) 50-nm tannate coated Au MNMs (T-MNMs). No evidence was found indicating that the MNMs penetrated the plant root surface.

result of the longer exposure time for the tobacco. However, one recent study did not see any leaf translocation of MNMs in wheat after several months of exposure, albeit in soil,¹⁶ and our observation of almost complete aggregation of the MNMs in the wheat treatments at the end of 3 d makes it unlikely that additional exposure time would have resulted in fundamentally different results. Additionally, Nedoskin et al. recently used in vivo plant flow cytometry to demonstrate that uptake of CNT-quantum dot conjugates by tomato plants occurs within minutes.⁴⁶ We speculate that the differential bioaccumulation between the two plant species is likely the result of the differences in MNM aggregation induced in the treatment suspensions during the exposures and that these differences in aggregation are the result of root exudation of different compounds between the two plants. Wheat plants were observed to alkalinize their treatment suspensions to a greater degree than the tobacco plants in most treatments, although Ca and Mg exuded into the treatment suspensions by the two plant

species was not significantly different. Considering that increased alkalinization should have further stabilized the negatively charged MNMs, we cannot explain the increased aggregation observed in the wheat treatments.

In addition to potentially modifying the pH and concentrations of divalent cations in the rhizosphere, plant roots also exude many other solutes including mucilage, enzymes, sugars, phenolics, and amino acids that were not measured in this study, any of which could potentially affect MNM aggregation and bioavailability.¹⁷ As previously mentioned, in some cases, the differences between the exudates of monocots and dicots is dramatic. For example, monocots such as wheat exude amino acids such as mugineic acid in response to iron deficiency, whereas dicots such as tobacco exude phenolic and reducing compounds.¹⁷ Differences in the amount and nature of the exudation between species such as this could play a major role in inducing aggregation and affecting bioavailability of MNMs

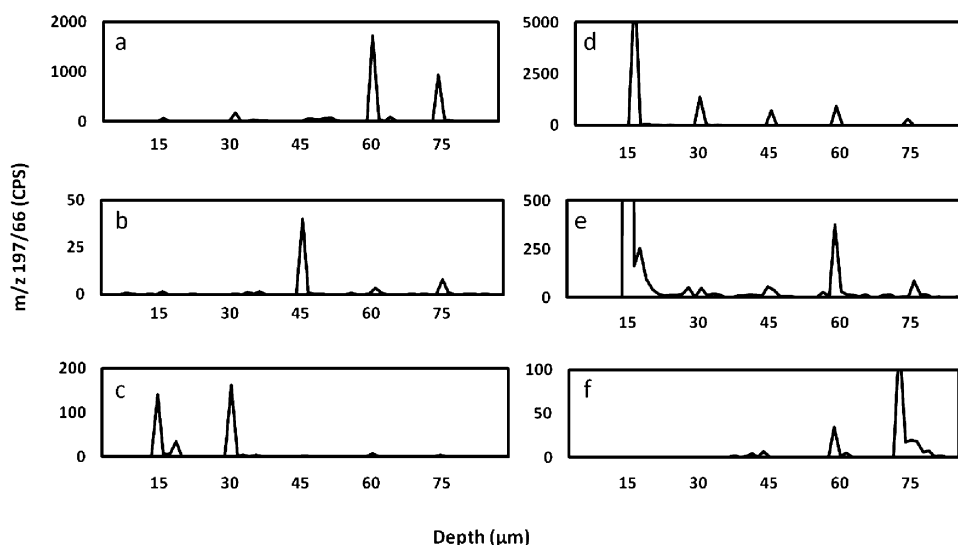


Figure 4. Laser ablation inductively coupled mass spectrometry (LA-ICP-MS) depth profiles from mesophyll of tobacco leaves exposed to (a) 10-nm, (b) 30-nm, and (c) 50-nm citrate coated manufactured Au nanomaterials (C-MNMs), and (d) 10-nm, (e) 30-nm, and (f) 50-nm tannate coated Au MNMs (T-MNMs). The presence of Au within leaf tissue removed during each laser burst demonstrates the presence of Au throughout the leaf. Au concentration reported as counts per second (CPS) of m/z 197 (Au) normalized by CPS for m/z 66 (Zn) to account for the mass of tissue removed from each laser burst.

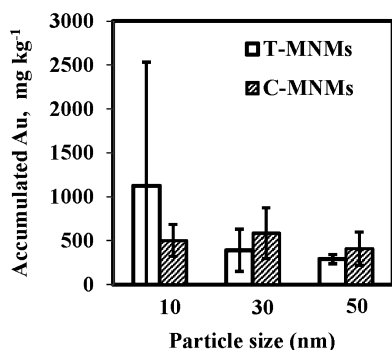


Figure 5. Bulk laser ablation inductively coupled plasma mass spectrometry (LA-ICP-MS) analysis of tobacco leaf tissue. Error bars represent SD. Treatments means were not significantly different from one another. T-MNMs = tannate coated manufactured nanomaterials (MNMs). C-MNMs = citrate coated MNMs.

and further investigation into this possibility represents an interesting area for future investigations.

This study presents some of the first data systematically examining the importance of particle size and MNM surface chemistry on the bioavailability of MNMs. Our data suggest that MNMs with a wide range of particle sizes and different surface coatings are bioavailable to plants in hydroponics and that MNMs do not need to passively move through cell wall pores to be taken up. However, it is likely that extrinsic properties imparted by soil components will influence uptake, possibly even affecting how MNM intrinsic properties affect uptake. Therefore, investigating the importance of MNM intrinsic properties to plant uptake in soil exposures is a necessary area of future research. We also observed large species-dependent differences in MNM bioaccumulation that we speculate are the ultimate result of differences in the nature of chemical root exudation between plant species. Given the lack of emphasis on studies focused on MNMs in terrestrial ecosystems to date, as well as evidence suggesting that MNMs can biomagnify in terrestrial food webs,¹² such information is

critical for developing an understanding of the mechanisms controlling plant uptake and the potential for trophic transfer of MNMs and will be required to help inform risk-based policy decisions on the regulation of nanomaterials.

■ ASSOCIATED CONTENT

📄 Supporting Information

TEM micrographs of nanoparticle suspensions, nanoparticle characterization data, characterization of treatment suspensions post exposure, XRF maps of wheat leaf tissues, plant germination protocols. This material is available free of charge via the Internet at <http://pubs.acs.org>.

■ AUTHOR INFORMATION

Corresponding Author

*Phone: 859-257-1651; e-mail: paul.bertsch@uky.edu; mail: University of Kentucky. Department of Plant and Soil Sciences N-212M, Agricultural Science Center, North Lexington, KY 40546.

Notes

The authors declare no competing financial interest.

■ ACKNOWLEDGMENTS

We acknowledge the advice and assistance of A. Lanzirrotti, R. Tappero, and A. Whitley. Major funding for this research was provided by the National Science Foundation (NSF) and the Environmental Protection Agency (EPA) under NSF Cooperative Agreement EF-0830093, Center for the Environmental Implications of NanoTechnology (CEINT). J.U. was supported by U.S. EPA through Science to Achieve Results Grant (RD 834857). This research was also partially supported by a grant from the U.S. Environmental Protection Agency's Science to Achieve Results (STAR) program (RD834574), the Transatlantic Initiative for Nanotechnology and the Environment. Any opinions, findings, conclusions or recommendations expressed in this material are those of the author(s) and do not necessarily reflect the views of the NSF or the EPA. This work has not been subjected to NSF or EPA review and no

official endorsement should be inferred. Portions of this work were performed at Beamline X26A, National Synchrotron Light Source (NSLS), Brookhaven National Laboratory. X26A is supported by the Department of Energy (DOE) - Geosciences (DE-FG02-92ER14244 to The University of Chicago - CARS) and DOE - Office of Biological and Environmental Research, Environmental Remediation Sciences Division (DE-FC09-96-SR18546 to the University of Kentucky). Use of the NSLS was supported by DOE under Contract DE-AC02-98CH10886.

REFERENCES

- (1) Gottshalk, F.; Sonderer, T.; Scholz, R. W.; Nowack, B. Modeled environmental concentrations of engineered nanomaterials (TiO₂, ZnO, Ag, CNT, Fullerenes) for different regions. *Environ. Sci. Technol.* **2009**, *43* (24), 9216–9222.
- (2) Kaegi, R.; Voegelin, A.; Sinnert, B.; Zuleeg, S.; Hagendorfer, H.; Burkhardt, M.; Siegrist, H. Behavior of metallic silver nanoparticles in a pilot wastewater treatment plant. *Environ. Sci. Technol.* **2011**, *45*, 3902–3908.
- (3) Kiser, M. A.; Westerhoff, P.; Benn, T.; Wang, Y.; Perez-Rivera, J.; Hristovski, K. Titanium nanomaterial removal and release from wastewater treatment plants. *Environ. Sci. Technol.* **2009**, *43*, 6757–6763.
- (4) Benn, T.; Westerhoff, P. Nanoparticle silver released into water from commercially available sock fabrics. *Environ. Sci. Technol.* **2008**, *42*, 4133–4139.
- (5) Limbach, L.; Bereiter, R.; Müller, E.; Krebs, R.; Gälli, R.; Stark, W. J. Removal of oxide nanoparticles in a model wastewater treatment plant: influence of agglomeration and surfactants on clearing efficiency. *Environ. Sci. Technol.* **2008**, *42*, 5828–5833.
- (6) Urine, J. M.; Bertsch, P. M.; Hunyadi, S. E. In *Nanoscience and Nanotechnology: Environmental and Health Impacts*; Grassian, V. H., Ed.; John Wiley and Sons, Inc: New York, 2008; pp 345.
- (7) Zhu, H.; Han, J.; Xiao, J.; Jin, Y. Uptake, translocation, and accumulation of manufactured iron oxide nanoparticles by pumpkin plants. *J. Environ. Monit.* **2008**, *10*, 713–717.
- (8) Lee, W.; An, Y. J.; Yoon, H.; Kweon, H. S. Toxicity and bioavailability of copper nanoparticles to the terrestrial plants mung bean (*Phaseolus radiatus*) and wheat (*Triticum aestivum*): plant agar test for water-insoluble nanoparticles. *Environ. Toxicol. Chem.* **2007**, *27* (9), 1915–1921.
- (9) Lin, S.; Reppert, J.; Hu, Q.; Hudson, J. S.; Reid, M. L.; Ratnikova, T. A.; Rao, A. M.; Luo, H.; Ke, P. C. Uptake, translocation, and transmission of carbon nanomaterials in rice plants. *Small* **2009**, *5* (10), 1128–1132.
- (10) Kurepa, J.; Paunesku, T.; Vogt, S.; Arora, H.; Rabatic, B. M.; Lu, J.; Wanzer, M. B.; Woloschak, G. E.; Smalle, J. A. Uptake and distribution of ultrasmall anatase TiO₂ alizarin red s nanoconjugates in *Arabidopsis thaliana*. *Nano Lett.* **2010**, DOI: 10.1021/nl903518f.
- (11) Sabo-Attwood, T.; Urine, J. M.; Stone, J. W.; Murphy, C. J.; Ghoshroy, S.; Blom, D.; Bertsch, P. M.; Newman, L. A. Uptake, distribution and toxicity of gold nanoparticles in tobacco (*Nicotiana xanthi*) seedlings. *Nanotoxicology* **2011**, *6* (4), 353–360, DOI: 10.3109/17435390.2011.579631.
- (12) Judy, J. D.; Urine, J. M.; Bertsch, P. M. Evidence for biomagnification of gold nanoparticles within a terrestrial food chain. *Environ. Sci. Technol.* **2011**, *45* (2), 776–781.
- (13) Yin, L.; Cheng, Y.; Espinasse, B.; Colman, B. P.; Auffan, M.; Wiesner, M.; Rose, J.; Liu, J.; Bernhardt, E. More than the ions: The effect of silver nanoparticles on *Lolium multiflorum*. *Environ. Sci. Technol.* **2011**, *45*, 2360–2367.
- (14) Lin, D.; Xing, B. Root uptake and phytotoxicity of ZnO nanoparticles. *Environ. Sci. Technol.* **2008**, *42*, 5580–5585.
- (15) Birbauium, K.; Brogioli, R.; Schellenberg, M.; Stark, W.; Gunther, D.; Limbach, L. No evidence for cerium dioxide nanoparticle translocation in maize plants. *Environ. Sci. Technol.* **2010**, *44*, 8718–8723.
- (16) Du, W.; Sun, Y.; Ji, R.; Zhu, J.; Wu, J.; Guo, H. TiO₂ and ZnO nanoparticles negatively affect wheat growth and soil enzyme activities in agricultural soil. *J. Environ. Monit.* **2011**, *13*, 822–828.
- (17) Marschner, H. *Mineral Nutrition of Higher Plants*; Academic Press: San Diego, CA, 1995.
- (18) Jia, G.; Wang, H.; Yan, L.; Wang, X.; Pei, J.; Yan, T.; Zhao, Y.; Guo, X. Cytotoxicity of Carbon Nanomaterials: Single-wall nanotube, multi-wall nanotube, and fullerene. *Environ. Sci. Technol.* **2005**, *39*, 1378–1383.
- (19) Chithrani, B.; Ghazani, A. A.; Chan, W. C. W. Determining the size and shape dependence of gold nanoparticle uptake into mammalian cells. *Nano Lett.* **2006**, *6* (4), 662–668.
- (20) Magrez, A.; Kasas, S.; Salicio, V.; Pasquier, N.; Seo, J. W.; Celio, M.; Catsicas, S.; Schwaller, B.; Forró, L. Cellular toxicity of carbon-based nanomaterials. *Nano Lett.* **2006**, *6* (6), 1121–1125.
- (21) Zhu, R. R.; Wang, S. L.; Chao, J.; Shi, D. L.; Zhang, R.; Sun, X. Y.; Yao, S. D. Bio-effects of Nano-TiO₂ on DNA and cellular ultrastructure with different polymorph and size. *Mater. Sci. Eng., C* **2009**, *29*, 691–696.
- (22) Carpita, N. Determination of the pore size of cell walls of living plant cells. *Science* **1979**, *205* (4411), 1144–1147.
- (23) El-Sayed, I.; Huang, X.; El-Sayed, M. A. Surface plasmon resonance scattering and absorption of anti-EGFR antibody conjugated gold nanoparticles in cancer diagnostics: applications in oral cancer. *Nano Lett.* **2005**, *5* (5), 829–834.
- (24) Bowman, M.; Ballard, T. E.; Ackerson, C. J.; Feldhein, D. L.; Margolis, D. M.; Melander, C. Inhibition of HIV fusion with multivalent gold nanoparticles. *J. Am. Chem. Soc.* **2008**, *130*, 6896–6897.
- (25) Kim, B. W.; Voitl, T.; Rodriguez-Rivera, J. G.; Dumesic, J. A. Powering fuel cells with CO via aqueous polyoxometalates and gold catalysts. *Science* **2004**, *305* (5688), 1280–1283.
- (26) Merchant, B. Gold, the noble metal and the paradoxes of its toxicology. *Biologicals* **1998**, *26* (1), 49–59.
- (27) Page, D. W.; van Leeuwen, J. A.; Spark, K. M.; Mulcahy, D. E. Pyrolysis characterisation of plant, humus and soil extracts from Australian catchments. *J. Anal. Appl. Pyrol.* **2002**, *65*, 269–285.
- (28) Bedran-Russo, A. K. B.; Yoo, K. J.; Emal, K. C.; Pashley, D. H. Mechanical properties of tannic-acid-treated dentin matrix. *J. Dent. Res.* **2009**, *88*, 807–812.
- (29) Lin, D.; Liu, N.; Yang, K.; Lizhong, Z.; Xua, Y.; Sing, B. The effect of ionic strength and pH on the stability of tannic acid-facilitated carbon nanotube suspensions. *Carbon* **2009**, *47*, 2875–2882.
- (30) Schiffman, S. S.; Suggs, M. S.; Sostman, L.; Simon, S. A. Chorda tympani and lingual nerve responses to astringent compounds in rodents. *Physiol. Behav.* **1992**, *51* (1), 51–63.
- (31) Collander, R. The partition of organic compounds between higher alcohols and water. *Acta Chem. Scand.* **1951**, *5*, 774–780.
- (32) Weast, R. C. *Handbook of Chemistry and Physics*; The Chemical Rubber Co.: Cleveland, OH, 1969.
- (33) Gu, B.; Schmitt, J.; Chen, Z.; Llang, L.; McCarthy, J. Adsorption and desorption of natural organic matter on iron oxide: Mechanisms and models. *Environ. Sci. Technol.* **1994**, *28*, 38–46.
- (34) Li, Q.; Xie, B.; Hwang, Y.; Xu, Y. Kinetics of C₆₀ fullerene dispersion in water enhanced by natural organic matter and sunlight. *Environ. Sci. Technol.* **2009**, *43*, 3574–3579.
- (35) Raskin, I.; Nanda Kumar, P. B. A.; Dushenkov, S.; Salt, D. E. Bioconcentration of heavy metals by plants. *Curr. Opin. Biotechnol.* **2004**, *5*, 285–290.
- (36) Bravin, M. N.; Marti, A. L.; Clairotte, M.; Hinsinger, P. Rhizosphere alkalisation — a major driver of copper bioavailability over a broad pH range in an acidic, copper-contaminated soil. *Plant Soil* **2009**, *318*, 257–268.
- (37) Fleicher, A.; O'Neil, M. A.; Ehwald, R. The pore size of non-graminaceous plant cell walls is rapidly decreased by borate ester cross-linking of the pectic polysaccharide rhamnolacturonan. *Plant Physiol.* **1999**, *121*, 829–838.

- (38) Tepeer, M.; Taylor, I. The permeability of plant cell walls as measured by gel filtration chromatography. *Science* **1981**, *213* (4509), 761–763.
- (39) Adani, F.; Papa, G.; Schievano, A.; Cardinale, G.; D' Imporzano, G.; Tambone, F. Nanoscale structure of the cell wall protecting cellulose from enzyme attack. *Environ. Sci. Technol.* **2011**, *45*, 1107–1113.
- (40) Kim, K.; Sung, W. S.; Suh, B. K.; Moon, S.; Choic, J.; Kim, J. G.; Lee, D. G. Antifungal activity and mode of action of silver nanoparticles on *Candida albicans*. *Biometals* **2009**, *22*, 235–242.
- (41) Wild, E.; Jones, K. Novel method for the direct visualization of in vivo nanomaterials and chemical interactions in plants. *Environ. Sci. Technol.* **2009**, *43*, 5290–5294.
- (42) Chen, R.; Ratnikova, T. A.; Stone, M. B.; Lin, S.; Lard, M.; Huang, G.; Hudson, J. S.; Ke, P. C. Differential uptake of carbon nanoparticles by plant and mammalian cells. *Small* **2010**, *6* (5), 612–617.
- (43) Liu, Q.; Chen, B.; Wang, Q.; Shi, X.; Xiao, Z.; Lin, J.; Fang, X. Carbon nanotubes as molecular transporters for walled plant cells. *Nano Lett.* **2009**, *9* (3), 1007–1010.
- (44) Yang, K.; Lin, D.; Xing, B. Interactions of humic acid with nanosized inorganic oxides. *Langmuir* **2009**, *25*, 3571–3576.
- (45) Illes, E.; Tombacz, E. The effect of humic acid adsorption on pH-dependent surface charging and aggregation of magnetite nanoparticles. *J. Colloid Interface Sci.* **2005**, *295*, 115–123.
- (46) Nedoskin, D. A.; Khodakovskaya, M. V.; Biris, A. S.; Wang, D.; Xu, Y.; Villagarcia, H.; Galanzha, E. I.; Zharav, V. P. *In vivo* plant flow cytometry: a first proof-of-concept. *Cytometry Part A* **2011**, *79A*, 855–865.